Highly Luminescent Organic−Inorganic Hybrid Mesoporous Silicas Containing Tunable Chemosensor inside the Pore Wall

Debraj Chandra,[†] Toshiyuki Yokoi,[‡] Takashi Tatsumi,[‡] and Asim Bhaumik*[,†]

Department of Materials Science and Centre for Advanced Materials, Indian Association for the Cultivation of Science, Jadavpur, Kolkata 700 032, India, and Catalytic Chemistry Division, Tokyo Institute of Technology, Midori-ku, Yokohama 226-8503, Japan

Received July 19, 2007

New multifunctional luminescent hybrid mesoporous silicas (LHMS) containing a tunable chemosensor diimine moiety inside the pore wall have been synthesized. XRD and TEM image analyses indicate the formation of highly ordered 2D hexagonal mesophase from a 1:3 mixture of diimine organosilica and tetraethyl orthosilicate (TEOS) assisted by the supramolecular assembly of cetyltrimethylammonium bromide (CTAB); the use of diimine organosilica precursor alone leads to disordered mesophase. ^{13}C CP MAS, ^{29}Si MAS NMR, and UV−visible spectroscopic data show the incorporation of bridging organic diimine in the solid mesoporous materials. N_2 sorption data suggest high BET surface areas together with type IV isotherms for the LHMS samples. These hybrid mesoporous materials show very strong affinity for metal cations (Fe^{3+}, Zn^{2+}, etc.), which could be utilized for possible application to metal ion chemosensors. All the LHMS samples exhibit very strong photoluminescence at room temperature and strong dependence of emission on exogenous ions. The highly ordered sample has the advantage over the disordered sample synthesized over pure diimine precursor, because its ion-exchange efficiency is high and it is synthesized with a small amount of diimine chemosensor precursor.

Introduction

Multifunctional nanostructured materials with ion-exchange, electrical, magnetic, and luminescent properties have great potential as chemical[1] and biological nanosensors,[2] optoelectronic nanodevices,[3] and environmental cleanup.[4] Fluorescent chemosensors[5] of nanoscale dimensions that can sense metal ions from solution have attracted particular attention these days because of their applications in display devices,[6] biological probes,[7] and novel light-emitting materials.[8] However, the luminescence property of most of these fluorescent chemical sensors has been examined in either organic solvent[5] or polymeric matrices with low surface area.[9] Although the tunable fluorophores have attracted considerable interest in recent years as chemosensors, highly emissive tunable chromophores in the solid state are extremely rare. A unique approach to controlling the emitted color from the solid materials is to incorporate a moiety functioning as a fluorescent chemosensor[10] into an organic−inorganic hybrid periodic mesoporous silica (PMO).[11−13] PMOs and related silica-based hybrid materials[11−16] have been synthesized from an organosilane compound ($(R'O)_3Si-R-Si(OR')_3$, R = CH_2CH_2, C_6H_4, etc., R′ = CH_3, C_2H_5, etc.) having two

* Corresponding author. E-mail: msab@mahendra.iacs.res.in.
[†] Indian Association for the Cultivation of Science.
[‡] Tokyo Insitute of Technology.

(1) (a) Leclerc, M. *Adv. Mater*. **1999**, *11*, 1491. (b) Kim, J.; Lee, J. E.; Lee, J.; Yu, J. H.; Kim, B. C.; An, K.; Hwang, Y.; Shin, C.-H.; Park, J.-G.; Kim, J.; Hyeon, T. *J. Am. Chem. Soc*. **2006**, *128*, 688. (c) Ravindranath, R.; Ajikumar, P. K.; Hanafiah, N. B. M.; Knoll, W.; Valiyaveettil, S. *Chem. Mater.* **2006**, *18*, 1213.
(2) (a) Schnadt, J.; Brühwiler, P. A.; Patthey, L.; O'Shea, J. N.; Södergren, S.; Odelius, M.; Ahuja, R.; Karis, O.; Bässler, M.; Persson, P.; Siegbahn, H.; Lunell, S.; Mårtensson, N. *Nature* **2002**, *418*, 620. (b) Zhao, X.; Tapec-Dytioco, R.; Tan, W. *J. Am. Chem. Soc.* **2003**, *125*, 11474.
(3) (a) Chen, X.; Rogach, A. L.; Talapin, D. V.; Fuchs, H.; Chi, L. *J. Am. Chem. Soc*. **2006**, *128*, 9592. (b) Song, C. S. *Catal. Today* **2006**, *115*, 2.
(4) (a) Huo, Q. S.; Zhao, D.; Feng, J. L.; Weston, K.; Buratto, S. K.; Stucky, G. D.; Schacht, S.; Schüth, F. *Adv. Mater*. **1997**, *9*, 974. (b) Arkas, M.; Tsiourvas, D.; Paleos, C. M. *Chem. Mater*. **2005**, *17*, 3439. (c) Subramanian, V.; Roeder, R. K.; Wolf, E. E. *Ind. Eng. Chem. Res.* **2006**, *45*, 2187. (d) Sayari, A.; Hamoudi, S.; Yang, Y. *Chem. Mater*. **2005**, *17*, 212.
(5) (a) Joshi, H. S.; Jamshidi, R.; Tor, Y. *Angew. Chem., Int. Ed*. **1999**, *38*, 2721. (b) Hwang, G. T.; Son, H. S.; Ku, J. K.; Kim, B. H. *J. Am. Chem. Soc*. **2003**, *125*, 11241.
(6) (a) Martinez-Manez, R.; Sancenon, F. *Chem. Rev.* **2003**, *103*, 4419. (b) Camerel, F.; Bonardi, L.; Schmutz, M.; Ziessel, R. *J. Am. Chem. Soc*. **2006**, *128*, 4548.
(7) Michalet, X.; Weiss, S.; Jager, M. *Chem. Rev.* **2006**, *106*, 1785.
(8) (a) Jenekhe, S. A. *Adv. Mater*. **1995**, *7*, 309. (b) Hide, F.; Diaz-Garcia, M. A.; Schartz, B. J.; Heeger, A. J. *Acc. Chem. Res*. **1997**, *30*, 430. (c) Kraft, A.; Grimsdale, A. C.; Holmes, A. B. *Angew. Chem., Int. Ed.* **1998**, *37*, 402. (d) Yamaguchi, Y.; Ochi, T.; Miyamura, S.; Tanaka, T.; Kobayashi, S.; Wakamiya, T.; Matsubara, Y.; Yoshida, Z.-i. *J. Am. Chem. Soc*. **2006**, *128*, 4504.
(9) (a) Berggren, M.; Inganas, O.; Gustafsson, G.; Rasmusson, J.; Andersson, M. R.; Hjertberg, T.; Wennerstrom, O. *Nature* **1994**, *372*, 444. (b) Dähne, L.; Biller, E.; Baumgärtel, H. *Angew. Chem., Int. Ed*. **1998**, *37*, 646. (c) Trenor, S. R.; Shultz, A. R.; Love, B. J.; Long, T. E. *Chem. Rev.* **2004**, *104*, 3059.
(10) Krämer, R. *Angew. Chem., Int. Ed.* **1998**, *37*, 772.
(11) (a) Inagaki, S.; Guan, S.; Fukushima, Y.; Ohsuna, T.; Terasaki, O. *J. Am. Chem. Soc*. **1999**, *121*, 9611. (b) Inagaki, S.; Guan, S.; Ohsuna, T.; Terasaki, O. *Nature* **2002**, *416*, 304.
(12) (a) Asefa, T.; MacLachlan, M. J.; Coombs, N.; Ozin, G. A. *Nature* **1999**, *402*, 867. (b) Asefa, T.; Kruk, M.; MacLachlan, M. J.; Coombs, N.; Grondey, H.; Jaroniec, M.; Ozin, G. A. *J. Am. Chem. Soc.* **2001**, *123*, 8520.
(13) (a) Melde, B. J.; Holland, B. T.; Blanford, C. F.; Stein, A. *Chem. Mater*. **1999**, *11*, 3302. (b) Stein, A.; Melde, B. J.; Schroden, R. C. *Adv. Mater*. **2000**, *12*, 1403.
(14) (a) Sayari, A.; Hamoudi, S. *Chem. Mater*. **2001**, *13*, 3151. (b) Anwander, R. *Chem. Mater*. **2001**, *13*, 4419. (c) Vinu, A.; Hossain, K. Z.; Ariga, K. *J. Nanosci. Nanotechnol*. **2005**, *5*, 347.

10.1021/cm701918t CCC: $37.00
Published on Web 10/06/2007

trialkoxysilyl groups connected by an organic bridge. These materials have a homogeneous distribution of organic fragments and silica moieties within the framework, which can be designed to carry chiral[17] or bulky functionalities.[18−20] The unique structural features of these materials make them potentially useful in a wide range of advanced applications, such as selective separation, sensing, catalysis,[21] optoelectronics,[22] low-*k* dielectric[23] materials, etc. Thus, ideally, by chemically grafting a fluorophore into the pore walls of the mesoporous silica materials, one would be able to tune these materials' photophysical characteristics externally as desired.

During the past decade, much interest has been focused on the development of solid-state optical emitters.[24] These molecules are extremely photostable and exhibit strong nonlinear optical effects. Diimine analogues possess a number of unique properties due to an extensive delocalized π-system.[25] The excellent nucleophilic (electron donor) nature of diimine makes them interesting building blocks of more complex systems.[25,26] Incorporation of diimine groups into the walls of mesoporous silica is thus promising for its applications in electronics, optoelectronics, and nonlinear optics. Because phenolic diimine is a good electron donor, they may interact with electron acceptors such as transition metal cations through chelation; their corresponding metal complexes are well-known polymerization catalysts.[27,28]

Although there are a few reports on postsynthesis doping of luminescent dyes in zeolites[29,30] or anchoring fluorophore groups[31−33] in the surface of mesoporous silica[34,35] and their interesting photophysical properties,[36] to the best of our knowledge, photoluminescence properties due to the bridging organic moiety in PMOs have never been explored. Compared to anchoring fluorophore groups, which mainly exist at the pore surface, use of bridging organosilane is well-recognized as a better alternative because the fluorophore resides in a confined geometry in the pore wall of a high-surface-area matrix and hardly causes a steric hindrance to adsorption of guest molecules. Furthermore, compared to zeolites, it is much easier to incorporate organic moieties with luminescence properties into the pore wall of mesoporous materials. Herein, we first report a photoluminescent organic−inorganic hybrid mesoporous diimine-incorporated silica (LHMS), where a group functioning as a tunable chemosensor is covalently grafted into the mesopore walls. The emission wavelength can be further modulated by the addition of proton or metal cations. Because of the presence of chelating donor sites and existence of protonated/deporotonated states, these novel PMOs can show a unique sensing ability for a trace amount of a metal cation or proton. Thus, one mesoporous material can be utilized for the generation of various emission colors. The rigid framework of highly ordered 2D hexagonal mesoporous silica with very high surface area and high affinity toward various cations is an attractive feature when this tunable chemosensor is binded into the pore wall of a mesoporous material. The tunability of the emission band due to the incorporated bridging diimine unit toward exogenous ions (like proton and metal cations) is one of the remarkable new features of this work, which has not been reported in prior approaches to anchoring a fluorophore on the surface of mesoporous silica[33] or postsynthesis grafting on mesoporous solids used for anion recognition.[36]

Experimental Section

Synthesis of Schiff-Base-Bridged Fluorescent Organosilane Source (I). All the reactions were carried out in flame-dried glassware under an argon atmosphere. Na-distilled dry ethanol was used for synthesis. (3-Aminopropyl)triethoxysilane (APTES) was used as received from Aldrich. 2,6-Diformyl-4-methylphenol (DFP) was synthesized according to a literature procedure.[37] For the synthesis of the Schiff base,[38] a solution of DFP (6.56 g, 0.04 mole) in dry ethanol (75 mL) was placed under argon in a two-necked round-bottom flask equipped with a condenser and an addition

(15) (a) Yamamoto, K.; Sakata, T.; Nohara, Y.; Takahashi, Y.; Tatsumi, T. *Science* **2003**, *300*, 470. (b) Yamamoto, K.; Nohara, Y.; Domon, Y.; Takahashi, Y.; Sakata, Y.; Plévert, J.; Tatsumi, T. *Chem. Mater*. **2005**, *17*, 3913.
(16) Sarkar, K.; Laha. S. C.; Bhaumik, A. *J. Mater. Chem*. **2006**, *16*, 2439.
(17) Baleizão, C.; Gigante, B.; Das, D.; Alvaro, M.; Garcia, H.; Corma, A. *Chem. Commun.* **2003**, 1860.
(18) (a) Olkhovyk, O.; Jaroniec, M. *J. Am. Chem. Soc.* **2005**, *127*, 60. (b) Olkhovyk, O.; Pikus, S.; Jaroniec, M. *J. Mater. Chem.* **2005**, *15*, 1517.
(19) (a) Cornelius, M.; Hoffmann, F.; Froba, M. *Chem. Mater*. **2005**, *17*, 6674. (b) Grudzien, R. M.; Grabicka, B. E.; Pikus, S.; Jaroniec, M. *Chem. Mater*. **2006**, *18*, 1722.
(20) Lee, B.; Im, H. J.; Luo, H. M.; Hagaman, E. W.; Dai, S. *Langmuir* **2005**, *21*, 5372−5376.
(21) (a) Bhaumik, A.; Tatsumi, T. *J. Catal*. **2000**, *189*, 31. (b) Kapoor, M. P.; Bhaumik, A.; Inagaki, S.; Kuraokab, K.; Yazawa, T. *J. Mater. Chem.* **2002**, *12*, 3078. (c) Bhaumik, A.; Kapoor, M. P.; Inagaki, S. *Chem. Commun.* **2003**, 470. (d) Nakajima, K.; Tomita, I.; Hara, M.; Hayashi, S.; Domen, K.; Kondo, J. N. *Adv. Mater*. **2005**, *17*, 1839. (e) Benitez, M.; Bringmann, G.; Dreyer, M.; Garcia, H.; Ihmels, H.; Waidelich, M.; Wissel, K. *J. Org. Chem*. **2005**, *70*, 2315.
(22) (a) Mal, N. K.; Fujiwara, M.; Tanaka, T. *Nature* **2003**, *421*, 350. (b) Garcia, H. *Pure Appl. Chem*. **2003**, *75*, 1085. (c) Peng, H.; Tang, J.; Yang, L.; Pang, J.; Ashbaugh, H. S.; Brinker, C. J.; Yang, Z.; Lu, Y. *J. Am. Chem. Soc*. **2006**, *128*, 5304.
(23) (a) Yang, S.; Mirau, P. A.; Pai, C.-S.; Nalamasu, O.; Reichmanis, E.; Pai, J. C.; Obeng, Y. S.; Seputro, J.; Lin, E. K.; Lee, H. -J.; Sun, J.; Gidley, D. W.; *Chem. Mater*. **2002**, *14*, 369. (b) Hatton, B. D.; Landskron, K.; Whitnall, W.; Perovic, D. D.; Ozin, G. A. *Adv. Funct. Mater*. **2005**, *15*, 823.
(24) Gustafsson, G.; Cao, Y.; Treacy, G. M.; Klavetter, F.; Colaneri, N.; Heeger, A. J. *Nature* **1992**, *357*, 477.
(25) Gobel, A.; Leibeling, G.; Rudolph, M.; Imhof, W. *Organometallics* **2003**, *22*, 759.
(26) Saito, T.; Yamada, T.; Miyazaki, S.; Otani, T. *Tetrahedron Lett.* **2004**, *45*, 9585.
(27) Pelascini, F.; Peruch, F.; Lutz, P. J.; Wesolek, M.; Kress, J. *Eur. Polym. J*. **2005**, *41*, 1288.
(28) Small, B. L.; Brookhart, M. *Macromolecules* **1999**, *32*, 2120.
(29) (a) Knops-Gerrits, P.-P. H. J. M.; De Schryver, F. C.; Van Der Auweraer, M.; Van Mingroot, H.; Li, X. −Y.; Jacobs, P. A. *Chem.—Eur. J.* **1996**, *2*, 592. (b) Calzaferri, G.; Huber, S.; Maas, H.; Minkowski, C. *Angew. Chem., Int. Ed.* **2003**, *42*, 3732.
(30) Comes, M.; Marcos, M. D.; Martínez-Máñez, R.; Millán, M. C.; Ros-Lis, R. V.; Sancenón, F.; Soto, J.; Villaescusa, L. A. *Chem.—Eur. J.* **2006**, *12*, 2162.
(31) Sanchez, C.; Lebeau, B.; Chaput, F.; Boilot, J. P. *Adv. Mater*. **2003**, *15*, 1969.
(32) Fiorilli, S.; Onida, B.; Barolo, C.; Viscardi, G.; Brunel, D.; Garrone, E. *Langmuir* **2007**, *23*, 2261.
(33) Descalzo, A. B.; Marcos, M. D.; Martinez-Manez, R.; Soto, J.; Beltran, D.; Amoros, P. *J. Mater. Chem.* **2005**, *15*, 2721.
(34) Kresge, C. T.; Leonowicz Roth, W. J.; Vartuli, J. C.; Beck, J. S. *Nature* **1992**, *359*, 710.
(35) Wight, A. P.; Davis, M. E. *Chem. Rev*. **2002**, *102*, 3589.
(36) Casas, R.; Aznar, E.; Marcos, M. D.; Martinez-Manez, R.; Sancen, F.; Soto, J.; Amor, P. *Angew. Chem., Int. Ed*. **2006**, *45*, 6661.
(37) Verani, C. N.; Rentschler, E.; Weyhermüller, T.; Bill, E.; Chaudhuri, P. *J. Chem. Soc., Dalton Trans.* **2000**, *3*, 251.
(38) (a) van den Ancker, T. R.; Cave, G. W. V.; Raston, C. L. *Green Chem*. **2006**, *8*, 50. (b) Chandra, D.; Bhaumik, A. *Microporous Mesoporous Mater*. **2007**, *101*, 348.

Scheme 1. Schematic Diagram for the Synthesis of Fluorescent Silica Precursor

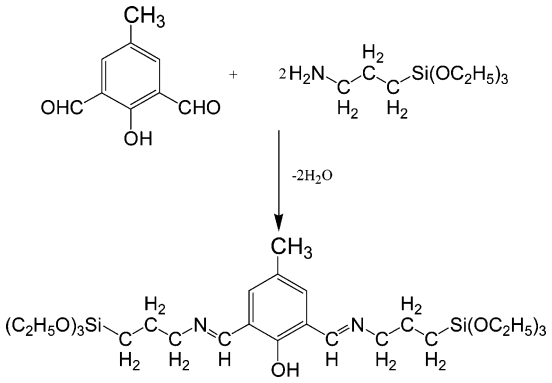

I

funnel. A solution of APTES (17.68 g, 0.08 mol) in dry ethanol (50 mL) was added dropwise over 30 min. Within 5 min after initiating the addition, the reaction became mildly exothermic. The reaction mixture was kept at reflux for 1 h after the completion of the addition of APTES. The mixture was allowed to cool to room temperature. Anhydrous Na_2SO_4 (40 g, Loba Chemie, India) was added to the mixture and the mixture was shaken for 15 min and then quickly filtered under argon to produce a clear, bright orange solution. Ethanol was removed from the solution in vacuum, leaving a highly viscous dark orange liquid. The as-synthesized bridged fluorescent organosilane precursor was designated as **I** (Scheme 1), which was highly sensitive to moisture. **I** was characterized by ^{1}H ^{13}C NMR, FT IR, and HRMS.[39]

Synthesis of Luminescent Hybrid Mesoporous Silica (LHMS). **I** and tetraethyl orthosilicate (TEOS, Aldrich) were used as fluorescent diimine organosilica and pure silica sources, respectively. Tartaric acid (TA, Loba Chemie) was used to adjust the initial pH of the mixture. Cetyltrimethylammonium bromide (CTAB, Loba Chemie) was used for structure direction. In a typical synthesis of sample 3, 2.40 g of CTAB (0.0066 mole) was dissolved in an aqueous solution of TA (0.66 g TA in 33 g of H_2O) under vigorous stirring at room temperature for 0.5 h. A premixed solution of **I** (1.90 g, 0.0033 mole) and TEOS (2.08 g, 0.01 mole) in 5 g of dry ethanol was then added dropwise to the mixture under continuous stirring for 0.5 h. After 2 h of continuous stirring, tetraethylammonium hydroxide (TEAOH, 35% aqueous, Demi Chem, India) was added dropwise into the mixture and the pH was maintained at ca. 11.0. The resulting mixture was kept under stirring for another 4 h at room temperature and then thermally treated at 353 K for 72 h under static conditions. The orange yellow solid was recovered by filtration, washed several times with water, and dried under a vacuum. Similar synthetic procedures were employed for the synthesis of the other two samples. The molar ratios of the constituents in the synthesis gels were

$$\mathbf{I}\text{:TEOS:CTAB:TA:}H_2O = 1\text{:}x\text{:}(1+x)/2\text{:}(1+x)/3\text{:}(1+x)138\ (x = 0, 1.0, \text{and } 3.0)$$

LHMS sample synthesized with pure **I** as silica source is designated as sample 1 and those synthesized with 1:1 and 1:3 **I**:TEOS ratios are designated as samples 2 and 3, respectively. Surfactant CTAB was removed from the as-synthesized solids by repeating ethanol−HCl extraction twice at room temperature and these samples are designated as acid-treated samples. The protonated forms of each of these samples were prepared by treating the acid-treated template-free samples with 1N HCl and water. Treating the acid-treated sample with 1 M aqueous NH_3 solution in water resulted in the deprotonated sample. The metal-exchanged samples were prepared by treating the deprotonated samples with 0.1 N aqueous solutions of metal salts. By subtracting the final concentrations of the metal ion after exchange from the respective initial concentrations ion-exchange capacities were calculated.

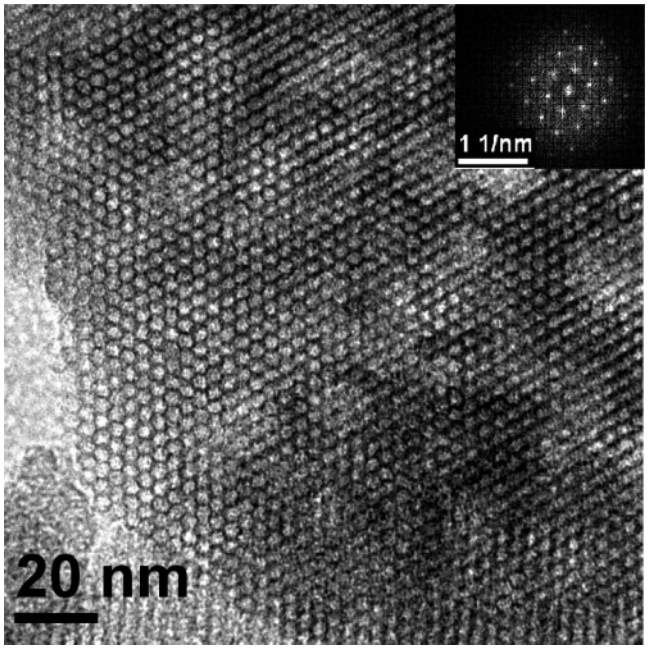

Figure 1. TEM image of sample 3.

Characterization Techniques. ^{1}H ^{13}C NMR experiments were carried out on a Bruker DPX-300 NMR spectrometer. FT IR spectra of these samples were recorded using a Nicolet MAGNA-FT IR 750 Spectrometer Series II. Mass spectrometric data were acquired by the electron spray ionization (ESI) technique at 25−70 eV in a Micromass Q-tof-Micro Quadruple mass spectrophotometer. Carbon, hydrogen, and nitrogen contents were analyzed using a Perkin-Elmer 2400 Series II CHN analyzer. X-ray diffraction patterns of the powder samples and the films were obtained with a Seifert P3000 diffractometer using Cu Kα (λ = 0.15406 nm) radiation. Nitrogen adsorption/desorption isotherms were obtained using a Quantachrome Autosorb 1C at 77 K. Prior to gas adsorption, all the samples were degassed for 2 h at 403 K. Transmission electron microscopic images were recorded on a JEOL 2010 TEM operated at 200 kV. A Hitachi S-5200 field-emission scanning electron microscope was used for the determination of the morphology of the particles. ^{13}C CP MAS and ^{29}Si MAS NMR studies were carried out on a JEOL-LA400WB 400 MHz spectrometer at resonance frequencies of 100.6 and 161.92 MHz, respectively. The chemical shifts for ^{29}Si spectra were referenced to TMS at 0 ppm. UV−visible diffuse reflectance spectra were recorded on a Shimadzu UV 2401PC with an integrating sphere attachment. $BaSO_4$ was used as background standard. The excitation and emission spectra were recorded on a Fluoromax-P Horiba Jobin-Yvon luminescence spectrometer, using a solid sample holder at room temperature. The powder samples were pressed to form a smooth, opaque flat disk for the optical study. Fluorescence lifetimes were determined by the time-resolved intensity decay method of time-correlated single-photon counting by using an IBH nanoLED-07 instrument equipped

(39) ^{1}H NMR (300 MHz, $CDCl_3$) δ 0.65 (t, J = 8.3 Hz, 4H), 1.19 (t, J = 6.9 Hz, 18H), 1.79 (m, 4H), 2.25 (s, 3H), 3.58 (t, J = 6.5 Hz, 4H), 3.78 (q, J = 6.8 Hz, 12H), 7.39 (s, 2H), 8.48 (s, 2H). ^{13}C NMR (75 MHz, $CDCl_3$) δ 8.0 (2C), 9.2 (1C), 18.3 (6C), 20.2 (2C), 24.4 (2C), 58.3 (6C), 118.1 (2C), 127.3 (2C), 133.3 (1C), 159.5 (2C), 164.8 (1C). IR (KBr) ν 3400, 2974, 1639, 1460, 1166, 1076, 956 cm^{-1}. HRMS calcd for $C_{27}H_{50}N_2O_7Si_2$ [M^+ + H]: 571.3229. Found: 571.3225.

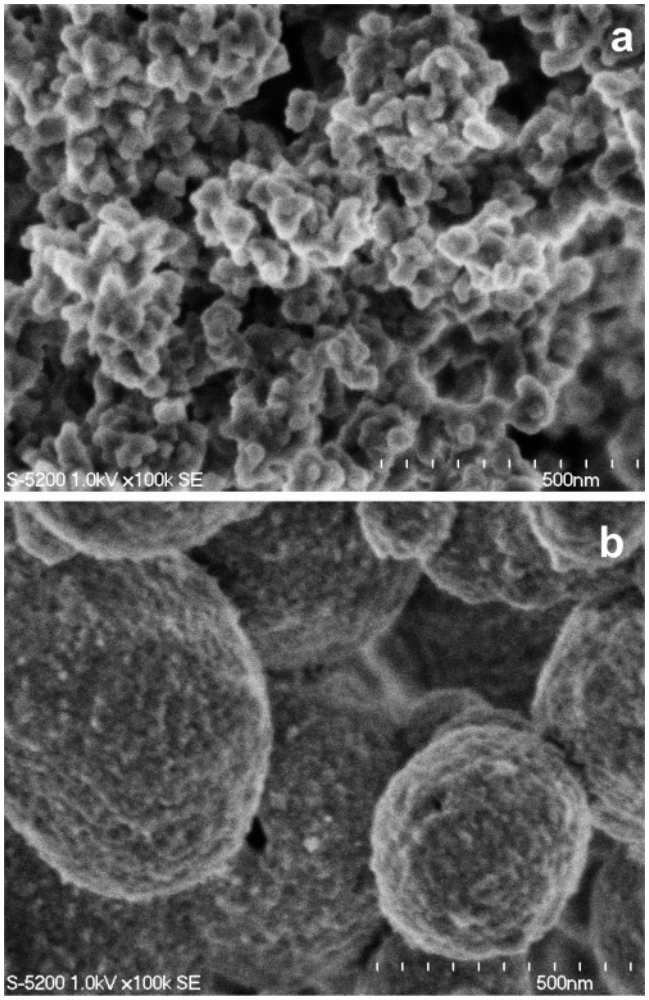

Figure 2. FE-SEM image of samples (a) 1 and (b) 3.

with a picosecond diode laser at 370 nm as light source. The typical response time of this laser system was 70 ps. The fluorescence decays were analyzed using an IBH DAS-6 instrument. Mean (average) fluorescence lifetime (τ) for biexponential iterative fitting were calculated from the decay times and the pre-exponential factors using the relation $\tau = a_1\tau_1 + a_2\tau_2$.

Results and Discussion

Characterizations of the Diimine Precursor. ^{1}H ^{13}C NMR, FT IR, and HRMS results indicated the formation of bridged fluorescent organosilane source (**I**)[39] as shown in Scheme 1. All the organic−inorganic hybrid LHMS samples were colored: yellow, light orange, yellowish orange, and deep orange for as-synthesized/deprotonated, protonated, Zn(II)-exchanged, and Fe(III)-exchanged samples, respectively. Pure diimine-silica (sample 1) showed more intense color than the samples 2 and 3 synthesized with the mixtures of **I** and TEOS. All three samples retained their colors after

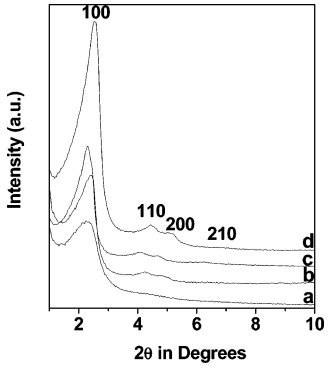

Figure 3. Powder XRD patterns of as-synthesized fluorescent hybrid mesoporous silica (a) sample 1 and (b) as-synthesized, (c) acid-treated, and (d) calcined sample 3.

treatments with acid or base. On the other hand, calcinations of these samples as well as the as-synthesized samples at 773 K for 4 h resulted in colorless mesoporous silica with no organic moiety.

HRTEM and FE-SEM. A TEM image of sample 3 is shown in Figure 1. In the image, low-electron-density spots (pores) were seen throughout the specimen, and the 2D hexagonal arrangement of the pores was quite clear. The electron diffraction pattern shown in the inset of this figure further suggested the 2D hexagonal structure for this LHMS sample. On the other hand, samples 1 and 2 with very high concentrations of **I** showed a disordered arrangement of pores (see the Supporting Information, Figures S1 and S2). SEM images of the LHMS samples 1 (a) and 3 (b) are shown in Figure 2. Whereas sample 1 synthesized with pure organosilane **I** as silica source consisted of small nanospheres of 30−50 nm (Figure 2a), sample 3 synthesized with a mixture of **I** and TEOS was composed of large spherical particles ca. 150−500 nm in diameter (Figure 2b). Thus, the morphology varied largely with the content of diimine-bridged silane; with the higher concentration of **I** in the synthesis gel, tinier particles were obtained.

Powder XRD. The powder X-ray diffraction patterns for as-synthesized LHMS materials are shown in Figure 3. Sample 3 (curves b−d) was highly ordered, showing strong three diffractions for the 100, 110, and 200 planes and a very weak one for the 210 plane of the 2D hexagonal mesophase.[11,24] Unit-cell parameters (a_0) were 4.32 and 4.13 nm for acid-treated and calcined samples, respectively. On the other hand, samples 1 (curve a) and 2 (see the Supporting Information, Figure S3) showed only one diffraction peaks corresponding to d = 3.81 and 3.76 nm, respectively, suggesting the formation of disordered mesostructured materials. All the samples retained their respective mesostructures and colors after the acid treatments and protonations. Interestingly, after calcination at 773 K, all the peaks

Table 1. Physicochemical Properties of LHMS Samples

sample no.	diimine:TEOS	BET surface area ($m^2\ g^{-1}$)	pore diameter[a] (nm)	pore volume (cc g^{-1})	Fe(III) IEC[b] (mequiv g^{-1})	Fe(III) IEE[c] (%)	Zn(II) IEC[b] (mequiv g^{-1})	Zn(II) IEE[c] (%)
1	∝	412	2.78	0.37	3.46	80.4	3.62	72.5
2	1:1	592	2.86	0.42	1.94	90.2	2.12	85.5
3	1:3	1140	2.88	0.59	1.42	99.1	1.65	100
3[d]		1418	3.10	0.80				

[a] Estimated by the KJS method.[40] [b] Ion-exchange capacity (IEC). [c] Ion-exchange efficiency (IEE). [d] Calcined at 773 K.

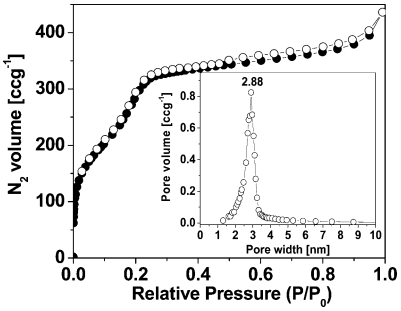

Figure 4. N_2 adsorption/desorption isotherms of sample 3. Adsorption points are marked by filled circles and desorption points by empty circles. KJS pore size distribution is shown in the inset.

for the 2D hexagonal mesostructure of sample 3 have been retained, as seen from the XRD pattern (Figure 3, curve 3d). One of the most unique features of these hybrid samples is that they retained their respective mesostructure and long-range ordering while the bulky diimine moiety was removed from the framework through the calcination process. This result agrees well with other organic−inorganic hybrid PMOs containing different organic spacers.[11−13]

N_2 Sorption. BET surface areas, average pore diameters, and pore volumes for LHMS samples estimated from their respective adsorption isotherms are given in Table 1. The N_2 adsorption/desorption isotherms of acid-treated sample 3 are shown in Figure 4. These isotherms were classified as type IV characteristic of the mesoporous materials.[11,34,35] The sharp increase in N_2 uptake for adsorption was observed at $P/P_0 = 0.24-0.32$, clearly indicating that the mesopores were uniform in size. Pore size distribution of this sample estimated by employing the KJS method[40] is shown in the inset of Figure 4. Acid-treated samples 1 and 2 also showed type IV isotherms (see the Supporting Information, Figures S4 and S5), suggesting the existence of mesopores. Thus the acid/ethanol extraction successfully removed the surfactants from the as-synthesized LHMS samples to generate mesoporosity. However, with the increase in the amount of diimine organosilica, the surface area remarkably decreased (Table 1, samples 3 and 1). This could be attributed to the loss in periodicity for sample 1 compared to sample 3. The BET surface area of acid-treated sample 3 increased to 1418 $m^2\ g^{-1}$ upon calcination.

^{13}C and ^{29}Si Solid-State MAS NMR. The ^{13}C CP MAS NMR spectrum for as-synthesized sample 1 (Figure 5) exhibits strong signals at 11.4, 20.4, 25.8, 57.8, 119.0, 123.3, 130.6, 133.5, 158.9, and 164.5 ppm because of the different carbon atoms of **I** as marked in the inset of Figure 5. This result indicates that the diimine fragment (**I**) was intact, being covalently linked to the silica inside the framework structure. Additional signals at 63.2 and 44.0 ppm in this spectrum, marked by asterisks (*) in this figure, could be attributed to the methyl groups and C_1 carbon atoms of the hexadecyl groups in the CTAB molecules.

^{29}Si MAS NMR spectra have been often used for assigning the chemical environment around the Si atoms in organic−inorganic hybrid silica-based materials.[11] Typical ^{29}Si MAS

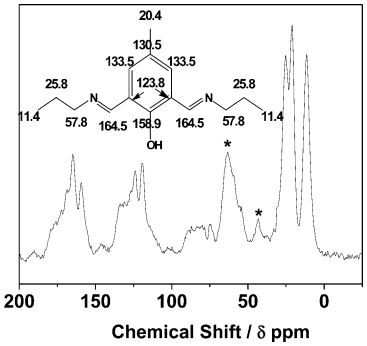

Figure 5. ^{13}C CP MAS NMR spectrum of LHMS, sample 1.

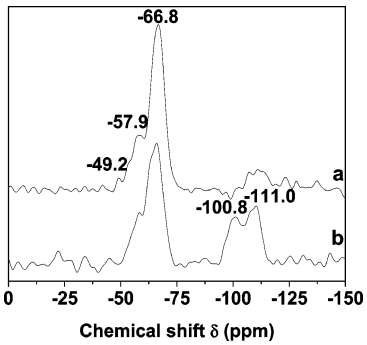

Figure 6. ^{29}Si MAS NMR spectra of LHMS samples (a) 1 and (b) 2.

NMR spectra of LHMS samples 1 and 2 are shown in Figure 6. Downfield chemical shifts at −66.8, −57.9, and −49.2 ppm were observed for sample 1, whereas for sample 2, signals at −111.0 and −100.8 ppm were observed in addition to those signals. This finding clearly indicated the incorporation of diimine bridges into the novel LHMS framework; for the ethylene-bridged hybrid mesoporous silica, ^{29}Si peaks with similar chemical shifts of ca. −66 ppm and −57 ppm corresponding to the T^3 ($(OSi)_3Si-R-Si(OSi)_3$) and T^2 ($(OH)_2(OSi)Si-R-Si(OSi)_2(OH)$) species, respectively, were observed.[11] Additional peaks at −111.0 and −100.8 ppm are attributed to the Q^4 and Q^3 silica species, indicating the presence of $Si(OSi)_n(OH)_{4-n}$ species for sample 2 synthesized with an equimolar ratio of **I** and TEOS.

Thermal Analyses. The quantitative determination of the diimine functional group contents in the surfactant-free LHMS samples was made by using thermogravimetic analysis (TGA) and differential thermal analysis (DTA) in a N_2 flow. The TGA and DTA profiles of the LHMS sample showed a first weight loss in the temperature range 298 to 373 K due to desorption of physisorbed water (about 6.5 wt %; see the Supporting Information, Figure S6). This was followed by a gradual decrease in the weight in the temperature range of 473−673 K by two steps, which corresponds to the loss of **I** fragments present in the pore wall. The total weight loss for the diimine group alone was about 43.6 wt % in the temperature range of 473−873 K, like other PMOs synthesized with different spacers.[11−14]

UV−vis Absorption. UV−visible spectroscopy was used for characterizing the optical absorbance of the diimine moiety present in the pore walls of the LHMS materials. Figure 7 shows the UV−visible diffuse reflectance spectra of derivatives of sample 1 (as-synthesized, protonated, deprotonated, and Fe(III)-exchanged and Zn(II)-exchanged

(40) (a) Kruk, M.; Jaroniec, M.; Sayari, A. *Langmuir* **1997**, *13*, 6267. (b) Jaroniec, M.; Solovyov, L. A. *Langmuir* **2006**, *22*, 6757.

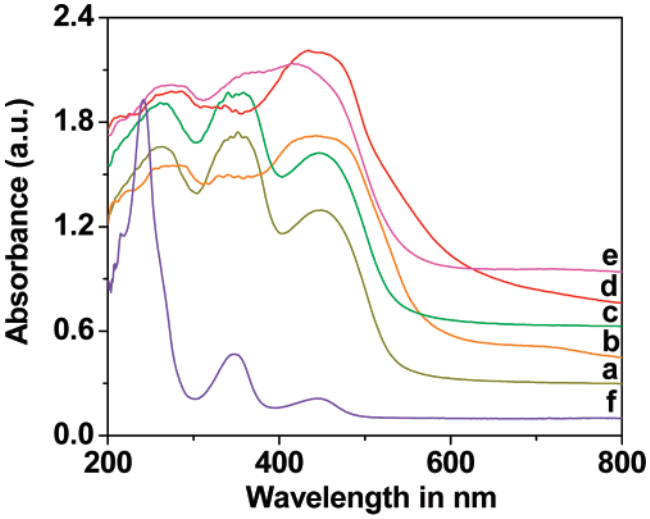

Figure 7. UV−vis diffuse reflectance spectra of LHMS sample 1: (a) as-synthesized, (b) protonated, (c) deprotonated, (d) Fe(III) exchanged, (e) Zn(II) exchanged, and (f) pure Schiff base **I**.

ones) as well as diimine precursor **I**. All these samples exhibited three major UV−visible absorption bands in the range of 200−600 nm. Diimine precursor **I** showed very strong absorption bands at 241 and 348 nm and a weak one at 448 nm. For Fe(III)- and Zn(II)-exchanged samples, a red shift of the absorption bands was observed. This could be attributed to the ligand chelation, which leads to ligand-to-metal charge transfer (LMCT) bands in addition to the $\pi \rightarrow \pi^*$ transitions due to the phenolic diimine.[41] Three strong absorption bands appeared at 261, 352, and 448 nm for the as-synthesized samples as well as the deprotonated samples. For the protonated sample, the band at 352 nm was suppressed. In the presence of acid, the imine-N gets protonated and thus their respective excited-state energy also changes. Metal complexes of diimine[41,42] also show three strong absorption bands in this UV−visible region.

Photoluminescence. The emission properties of the organic−inorganic hybrid LHMS samples are studied in the solid state at room temperature. Organic−inorganic composite materials often show emission spectra, which are largely dependent on the organic functionality.[43,44] Figures 8 and 9 show the photoluminescence (PL) excitation (A) and emission (B) spectra of the LHMS samples 1 and 3, respectively. Emission spectra of diimine precursor **I** and derivatives of samples 1 and 3 (as-synthesized, protonated, deprotonated, Fe(III)-exchanged, and Zn(II)-exchanged ones) are shown in these figures. All the samples showed a strong emission band between 500 and 590 nm upon excitation at 330−343 nm. (Figures 8 and 9A). The intensity for the PL excitation and emission spectra were almost equal, suggesting that these emission lines are due to the primary transition present in the functional groups of the materials. The emission spectra of Fe(III)- and Zn(II)-exchanged samples were distinctly red-shifted to higher wavelength with maxima

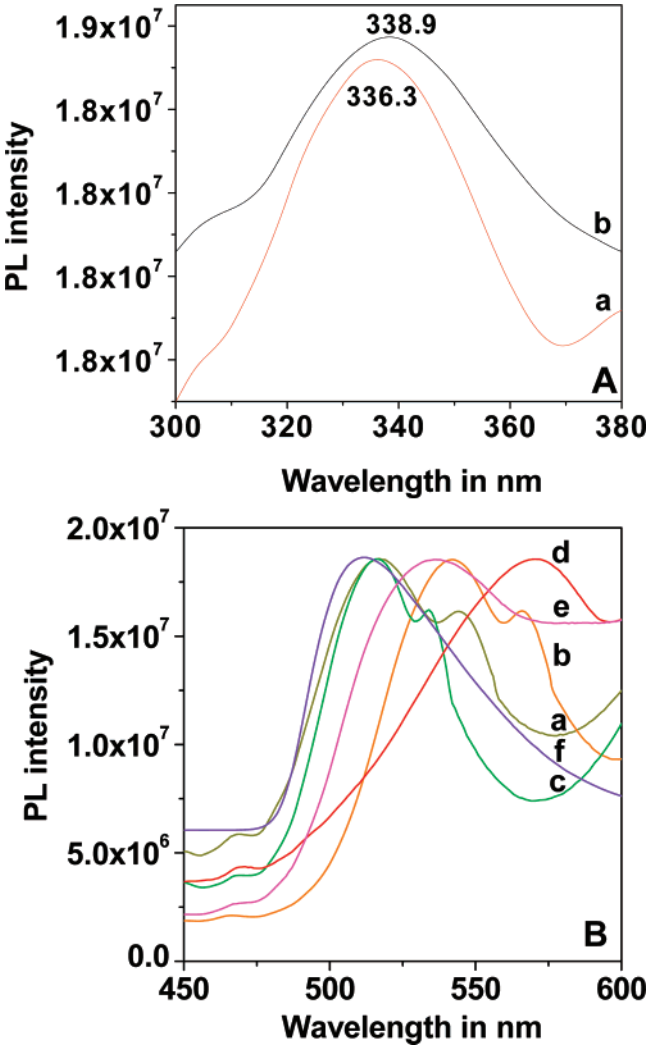

Figure 8. Photoluminescence spectra of LHMS sample 1: (A) excitation spectra of (a) as-synthesized, (b) protonated; (B) emission spectra of (a) as-synthesized, (b) protonated, (c) deprotonated, (d) Fe(III)-exchanged, (e) Zn(II)-exchanged, and (f) pure Schiff base **I** , excited at 340 nm.

at 570 and 536 nm, respectively, without substantial enhancement in intensity. Interestingly for all the samples, regardless of the concentration of the diimine moiety, multiple green to orange strong emission bands with maxima at ca. 516, 540, and 570 nm were observed upon excitation at 340 nm. Although precursor **I** showed single broad emission with a maximum at 512 nm, as-synthesized, protonated, and deprotonated samples showed bands at 534, 545, and 567 nm in addition to their respective major emission bands. For Fe(III)- and Zn(II)-exchanged samples these additional emission bands merged with the second harmonic of the excitation, and thus, we could not assign these relatively weak bands. The photophysical properties of the LHMS materials are unique in the sense that rare PMOs containing viologen[43] show electron-acceptor properties and that chiral organosilicas[44] in the presence of enantiomerically pure quenchers show photoluminescence properties.

Figure 10 shows emission images of deprotonated (1a), protonated (1b), Zn(II)-exchanged (1c), and Fe(III)-exchanged (1d) samples (sample 1) after UV light irradiation. Very strong fluorescence colors varying from pale green to

(41) Xiang, H.-F.; Chan, S.-C.; Wu, K. K.-Y.; Che, C.-M.; Lai, P. T. *Chem. Commun.* **2005**, 1408.
(42) Klare, J. E.; Tulevski, G. S.; Nuckolls, C. *Langmuir* **2004**, *20*, 10068.
(43) (a) Alvaro, M.; Ferrer, B.; Fornés, V.; García, H. *Chem. Commun.* **2001**, 2546. (b) Clennan, E. L. *Coord. Chem. Rev.* **2004**, *248*, 477.
(44) Alvaro, M.; Benitez, M.; Das, D.; Ferrer, B.; Garcia, H. *Chem. Mater.* **2004**, *16*, 2222.

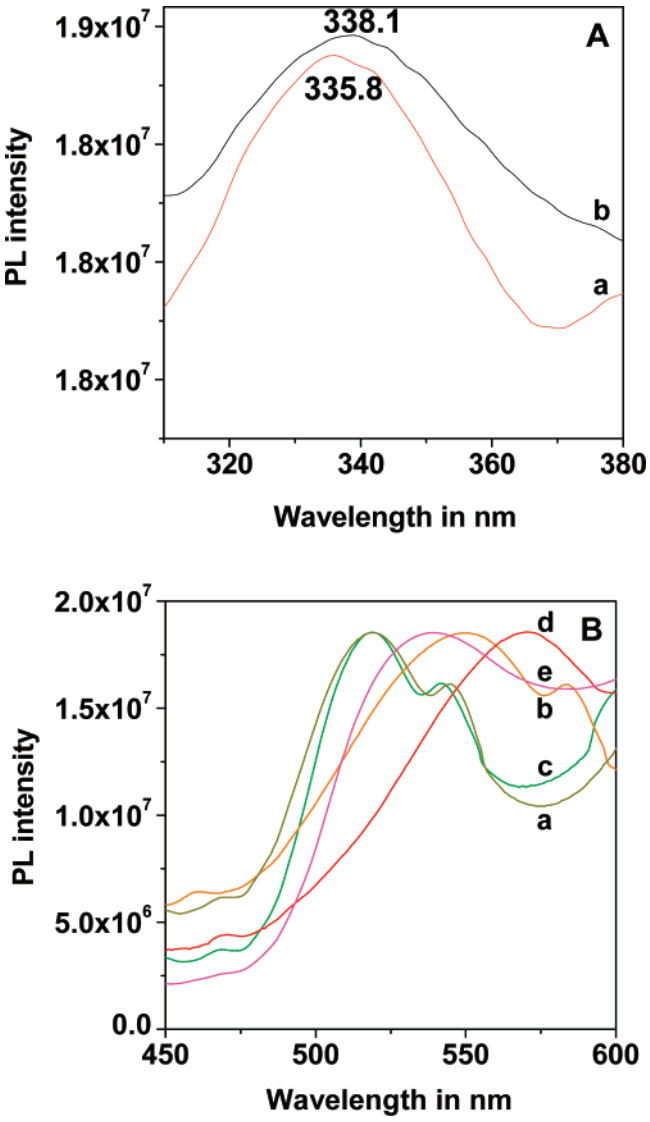

Figure 9. Photoluminescence spectra of LHMS sample 3: (A) excitation spectra of (a) as-synthesized, (b) protonated; (B) emission spectra of (a) as-synthesized, (b) protonated, (c) deprotonated, (d) Fe(III)-exchanged, (e) Zn(II)-exchanged, excited at 340 nm.

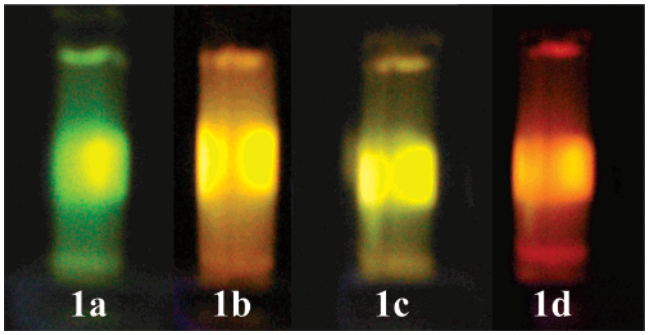

Figure 10. Photographic images of LHMS sample 1: (1a) deprotonated, (1b) protonated, (1c) Zn(II)-exchanged, and (1d) Fe(III)-exchanged after UV light irradiation.

bright orange emission were observed for all these LHMS samples. The optical properties of the LHMS samples are highly dependent upon the acid or base treatment (i.e., pH) and the effects of different metal cations (Fe^{3+} and Zn^{2+}) can be observed with the naked eye. On the basis of these results in Scheme 2, we propose the plausible structure **II** in the as-synthesized and deprotonated forms. On protonation

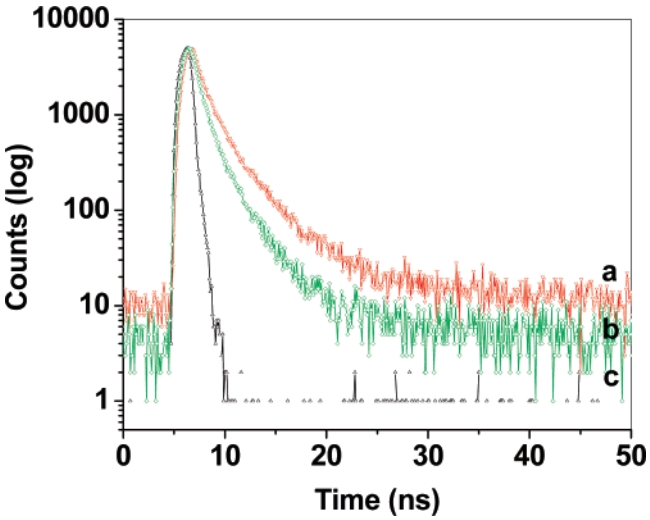

Figure 11. Time-resolved fluorescence decays of LHMS sample 1: (a) protnated, (b) deprotonated (λ_{ex} = 370 nm). The sharp profile (c) is the lamp profile.

Scheme 2. Model Structure for As-Synthesized or Deprotonated (II) and Protonated (III) LHMS Sample 1

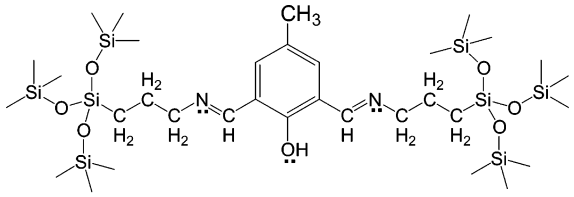

As-synthesised or deprotonated structure (II)

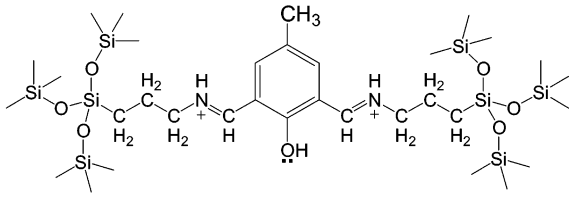

Protonated structure (III)

through acid treatment this yields species **III**, and in the presence of metal cation, the phenolic diimine moiety coordinates with metal cations, forming a chelating complex with phenolic OH and imine-N donors. Thus, the luminescence properties could be attributed to the $\pi \rightarrow \pi^*$ transition for **II** and **III** and to the LMCT complex formation in the presence of metal cations. It is pertinent to note that green to orange luminescence have been studied extensively because of their possible biological applications in sensors.[45]

Lifetime Measurements. Fluorescence lifetime, which is very sensitive to exited state interactions, can provide useful information for the local environment around a fluorophore moiety.[46] In the presence of neighboring silica species, the decay of **I** is biexponential, suggesting two different emissive pathways. This is responsible for multiple emission lines. In Figure 11, decay profiles of protonated and deprotonated samples are shown vis-à-vis the profile for the lamp (c). This figure suggests a typical biexponential decay profiles for the diimine chemosensor incorporated into the mesoporous silica

(45) Burns, A.; Ow, H.; Wiesner, U. *Chem. Soc. Rev.* **2006**, *35*, 1028.
(46) Mallick, A.; Haldar, B.; Chattopadhyay, N. *J. Phys. Chem. B* **2005**, *109*, 14683.

Table 2. Photophysical Properties of LHMS-1

sample name	a_1	τ_1 (ns)	a_2	τ_2 (ns)	τ^a (ns)	χ^2
LHMS-1-protonated	0.86	1.08	0.14	3.63	1.437	1.34
LHMS-1-deprotonated	0.88	0.83	0.12	2.49	1.029	1.202

[a] For all the lifetime measurements, the fluorescence decay curves were analyzed by biexponential iterative IBH fitting program.

pore wall. Table 2 shows photophysical parameters of fluorescence decays on protonated and deprotonated samples 1. The lifetimes for the protonated sample is found to be longer than those of pure and deprotonated samples. Short excited-state lifetimes (1−1.5 ns) for both cases suggest that the emitting excited-state is a singlet $\pi-\pi^*$ state.

Metal Exchange and Chelation. In Table, 1 ion-xchange capacity (IEC) and ion-exchange efficiency (IEE) of each sample for Fe(III) and Zn(II) are represented. As seen from the data, sample 3 synthesized from the least amount of diimine precursor showed maximum efficiency for the exchange/detection of metal cations. This could be attributed to highly ordered mesopores and much larger surface area for sample 3 than for samples 1 and 2. Phenolic diimine ligands have a strong affinity for the transition metal cations to form stable LMCT complexes, which enhances the interfacial electron-transfer rates[47] and thus reduces the band gap of these LHMS materials. Diimine ligands are known to form complexes with Fe(III).[27] In the LHMS samples, phenolic OH and the imine N-atoms located at the pore wall could be chelated by the metal cations when it comes into contact with the aqueous solution of the metal salts. Other PMOs containing cation[48] or anion[49] exchangable organic moieties also showed similar ion-exchange properties. The change in color and the nature of the absorption and emission spectra could be attributed to different structures of **II** and **III** because of the protonation of the nitrogen atoms of the diimine. The bridging diimine moiety has three donor sites, namely, two imine-N groups and one phenolic OH group. This could coordinate with the transition metal cations (Fe or Zn) via metal−ligand chelation. Our experimental data demonstrate that the chelating chemosensor moiety **I** should show great versatility toward exogenous ions, which may open new applications in the area of organic−inorganic hybrid mesoporous materials.[50]

Tunable Sensing Property. Further modulation of emission wavelengths is attained by the addition of proton or metal ions such as Fe^{3+} and Zn^{2+}. As shown earlier, Figure 8 illustrates the dramatic spectral changes of LHMS-1 upon the addition of different exogenous ions. Upon adding Zn^{2+} ions into a dispersion of the LHMS-1 in water, the emission color dramatically changed from bright green to yellow. A red shift of approximately 20 nm was observed upon addition of Zn^{2+} ions to the LHMS-1. A bright orange fluorescence, centered at 570 nm, was observed when LHMS-1 was treated with an aqueous Fe^{3+} solution. More profound red shifts were observed when strong acids were added to protonate the conjugated diimine ligands. Although the parent LHMS-1 exhibited a bright green emission centered at 516 nm, treatment of the LHMS-1 with 0.1 N HCl solution resulted in a shift of approximately 25 nm, and an evolution of an intense light orange emission centered at 541 nm. The combination of highly coordinating diimine functionality in the bridged organosilane precursor provides a unique method for tuning the intrinsic property of the fluorophores, where changes in the electronic polarization and coordination are translated into dramatic spectral changes.

Conclusions

Schiff base condensation between 2,6-diformyl-4-methylphenol with the primary amine group of 3-aminopropyltriethoxysilane yielded a bridged organosilane containing diimine and phenolic OH functionalities. We have prepared new organic−inorganic hybrid PMO materials by using this diimine Schiff base silica source under hydrothermal conditions through the supramolecular assembly of cationic surfactant CTAB. These organic−inorganic mesostructured composites showed uniform mesopores and considerably high BET surface areas and display tunable chemosensor property in the solid state. Very strong photoluminescence shown by these LHMS materials could be employed for its possible application in optical sensors. The chelation of Fe^{3+} and Zn^{2+} ions with the organic diimine and phenolic OH functionality present in the LHMS materials suggested its potential utility for sensing other metal cations and tune their emission spectra in the presence of exogenous ions. Apart from chemosensors, these unique photophysical properties of the LHMS materials could be utilized in light-harvesting and optoelectronic applications. Thus, the ability to functionalize the pore wall of a mesoporous material with a fluorescent chemosensor could open new avenues to the detection of trace elements, display devices, and biological probes as chemosensors as well as novel light-emitting materials.

Acknowledgment. A.B. thanks DST, New Delhi, for a Ramanna Fellowship grant. This work was partly funded by the NanoScience and Technology Initiative of DST. This work was also partly supported by a Core Research for Evolutional Science and Technology (CREST) of JST Corporation grant to T.T. The authors thank Dr. A. Patra and Prof. N. Chattopadhyay for helpful discussions.

Note Added after ASAP Publication. Reference 16 was modified in the version published ASAP October 6, 2007; the corrected version published ASAP October 10, 2007.

Supporting Information Available: Table I and Figures S1−S6 (PDF). This material is available free of charge via the Internet at http://pubs.acs.org.

CM701918T

(47) Moser, J.; Punchihewa, S.; Infelta, P. P.; Grätzel, M. *Langmuir* **1991**, *7*, 3012.
(48) Benitez, M.; Das, D.; Feira, R.; Pischel, U.; Garcia, H. *Chem. Mater*. **2006**, *18*, 5597.
(49) Lee, B.; Im, H. J.; Luo, H. M.; Hagaman, E. W.; Dai, S. *Langmuir* **2005**, *21*, 5372.
(50) Grudzien, R. M.; Pikus, S.; Jaroniec, M. *J. Phys. Chem. B* **2006**, *110*, 2972.